ELSEVIER

Neurobiology of Aging 31 (2010) 74–87

NEUROBIOLOGY OF AGING

www.elsevier.com/locate/neuaging

Altered expression and distribution of zinc transporters in APP/PS1 transgenic mouse brain

Li-Hong Zhang [a,b], Xin Wang [a], Zhi-Hong Zheng [a], Hao Ren [a], Meredin Stoltenberg [c], Gorm Danscher [c], Liping Huang [d], Ming Rong [a], Zhan-You Wang [a,*]

[a] *Department of Histology and Embryology, China Medical University, Shenyang 110001, PR China*
[b] *Department of Histology and Embryology, Liaoning University of Traditional Chinese Medicine, Shenyang 110032, PR China*
[c] *Department of Neurobiology, Institute of Anatomy, University of Aarhus, DK-8000 Aarhus C, Denmark*
[d] *USDA/ARS/Western Human Nutrition Research Center, Department of Nutrition and Rowe Program in Genetics, University of California at Davis, Davis, CA, USA*

Received 31 August 2007; received in revised form 19 February 2008; accepted 22 February 2008
Available online 3 April 2008

Abstract

Pathological accumulation of β-amyloid peptide (Aβ) is an early and common feature of Alzheimer's disease (AD). An increased zinc concentration can initiate the deposition of Aβ. The present study aimed to study the expression and distribution patterns of six members of the zinc transporter (ZnT) family, ZnT1, ZnT3, ZnT4, ZnT5, ZnT6, and ZnT7, in the APPswe/PS1dE9 transgenic mouse brain. Our results demonstrated a statistically significant ($P < 0.05$) increase of ZnT1, ZnT3, ZnT4, ZnT6, and ZnT7 in both hippocampus and neocortex using Western blot method and an abundant distribution of zinc ions in the plaques and amyloid angiopathic vessels using immersion autometallography. Furthermore, all ZnT immunoreactions were detected in most amyloid plaques and amyloid angiopathic vessels. ZnT1 and ZnT4 were extensively expressed in all parts of the plaques. ZnT3, ZnT5, and ZnT6 were expressed most prominently in the degenerating neurites in the peripheral part of the plaques, while ZnT7 was present in the core of the plaques. The amyloid angiopathic vessels showed a strong ZnT3 immunoreactivity. These results might suggest multiple roles of ZnTs in the deposition and organization of the Aβ composition.

Keywords: Zinc; Zinc transporter; Alzheimer's disease (AD); β-Amyloid peptide (Aβ); Cerebral amyloid angiopathy (CAA)

1. Introduction

Alzheimer's disease (AD) is a disease of progressive intellectual deterioration. It is pathologically characterized by neurofibrillary tangles (NFT) and senile plaques (SP). Another concomitant pathological change often seen in Alzheimer's disease is cerebral amyloid angiopathy (CAA), in which amyloid is deposited within the wall and in the vicinity of cerebral vessels. Aβ is generated from the amyloid precursor protein (APP) by a proteolytic activity of β- and γ-secretase (Kar et al., 2004). Pathological accumulation of Aβ is an early and common feature of AD.

Zinc, an essential trace element for mammals, is abundant in the nervous system and has been suggested to be involved in many biological functions (Vallee and Auld, 1993; Pérez-Clausell, 1996; Takeda, 2000a, 2001; Valente et al., 2002; Wang et al., 2004). In the brain, most zinc ions are tightly bound to macromolecules or serve as a cofactor for a large number of enzymes (Christianson, 1991; Coleman, 1992). Only 15–30% of total zinc is present as free or weakly bound zinc ions, and these zinc ions can be detected by zinc-staining techniques (Frederickson et al., 1987; Mancini et al., 1992; Takeda et al., 2000b; Miro-Bernie et al., 2003; Danscher et al., 2004). Aβ contains both high and low affinity zinc-binding sites, and zinc ions are the only physiologically available metal ions to precipitate Aβ at pH 7.4 (Bush et al., 1994a). Increase of zinc ions in the brain can trigger a deposition of Aβ that results in the formation of senile plaques (Bush et

* Corresponding author. Tel.: +86 24 23256666x5305; fax: +86 24 23256666x5305.
E-mail address: wangzy@mail.cmu.edu.cn (Z.-Y. Wang).

0197-4580/$ – see front matter © 2008 Elsevier Inc. All rights reserved.
doi:10.1016/j.neurobiolaging.2008.02.018

al., 1994b). Most likely this process is also responsible for the amyloid accumulations in the vessel walls of CAA. Metal chelating agents (clioquinol and DP-109, both membrane permeable chelators) have been shown to inhibit the formation of amyloid plaques in APP transgenic mouse brain (Cherny et al., 2001; Bush, 2002; Lee et al., 2004). Therefore, disruption of zinc homeostasis in the brain may be an early and necessary step in the initiation of Aβ accumulation.

Zinc cannot travel across biological membranes by passive diffusion. In mammals, two zinc transporter families (ZIP, SLC39 and ZnT, SLC30) are required for transporting zinc across the plasma membrane and distributing zinc around the cell (Eide, 2004; Palmiter and Huang, 2004). The ZIP family members are involved in uptake of zinc ions into the cell or release of stored zinc into the cytoplasm, while the ZnT family members are responsible for the extrusion of zinc outside the cytoplasm to the extracellular space or intracellular organelles (Colvin et al., 2003; Kambe et al., 2004). Until now, eight members of the ZnT family have been characterized and are referred to as ZnT1–8 (Palmiter et al., 1996a,b; Huang and Gitschier, 1997; Huang et al., 2002; Kirschke and Huang, 2003; Fabrice et al., 2004; Kambe et al., 2004; Seve et al., 2004). Two other ZnT genes, ZnT9 and ZnT10, have been predicted by the mouse and human genome resources (Sim and Chow, 1999; Seve et al., 2004). Most of the ZnTs, except for ZnT5, share six membrane-spanning domains and a histidine-rich intracellular loop between domains 4 and 5, which is believed to be the zinc-binding site.

Although zinc has been demonstrated to play an important role in the pathologic process of AD, the involvement of zinc transporter proteins in the regulation of zinc homeostasis of human and mouse AD brains is unclear. Recently, it has been reported that there are significant alterations in the expression of ZnT1 (Lovell et al., 2005), ZnT4, and ZnT6 (Smith et al., 2006) in human AD brains. However, a comprehensive description of the expression and distribution of zinc transporter proteins in the AD pathogenesis of APP/PS1 transgenic mouse brain has not been established. Analysis of zinc transporter protein expression patterns in the mouse AD brain will help to address the molecular mechanisms of zinc homeostasis involved in the AD pathogenesis. In the present study, we studied expression and distribution patterns of ZnT1 and ZnT3–7 in mouse normal and AD brains by immunofluorescence and Western blot analyses. In addition, the levels of free zinc ions in these brains were evaluated by immersion autometallography.

2. Materials and methods

2.1. Animals

Six male mice (three 9-month-old B6C3-Tg(APPswe, PSEN1dE9)85Dbo/J mice and three age-matched wild-type C57bl/6 mice) were used in this study (purchased from the Jackson Laboratory, USA). They were housed in a 12 h light/dark cycle at 21–22 °C and 50% humidity, with food and tap water available ad libitum. All experimental procedures were performed in agreement with the ethical standards of China Medical University. The animals were anaesthetized with sodium pentobarbital (50 mg/kg, i.p.) and decapitated. The brains were immediately removed and split in halves. One half of the brains were placed in 4% paraformaldehyde for immunofluorescence and immunohistochemistry analyses. The other half of the brains were cut into two slabs and were either placed in 3% glutaraldehyde for AMG analysis or frozen for Western blot assays.

2.2. Antibodies

All ZnT antibodies used in this study were affinity-purified rabbit antisera specific for each ZnT protein. ZnT1 antiserum was kindly provided by Dr. WF Silverman (Sekler et al., 2002); ZnT3 antiserum was kindly provided by Dr. RD Palmiter (Palmiter et al., 1996b); ZnT4–7 antisera were kindly provided by Dr. L Huang (Huang and Gitschier, 1997; Huang et al., 2002; Kirschke and Huang, 2003; Yu et al., 2007). The mouse monoclonal antibody detecting amino acid residues 1–12 of human Aβ was purchased from Sigma. GAPDH monoclonal antibody was purchased from Santa Cruz Biotechnology. Secondary antibodies, fluorescein isothiocyanate (FITC)-conjugated donkey anti-rabbit IgG, Texas Red-conjugated donkey anti-mouse IgG, and normal donkey serum (NDS), were purchased from Jackson ImmunoResearch Laboratory.

2.3. Tissue preparation for immunohistochemical and immunofluorescence staining

Fixed tissues were immersed in a series of ethanol solutions, increasing the concentration until absolute alcohol was reached. The tissues were then left in xylene overnight before being embedded in paraffin. Ten-micrometer-thick sections were cut, mounted on glass slides, kept overnight at 37 °C, and then at room temperature until use.

Prior to immunohistochemical and immunofluorescence staining, the sections were dewaxed in xylene and rehydrated through graded alcohols. They were then rinsed in 0.1 M Tris–HCl buffered saline (TBS, pH 7.4) and treated with 3% hydrogen peroxide (H_2O_2) in PB for 10 min to reduce endogenous peroxidase activity. After rinsing with TBS, the sections were boiled in a TEG buffer for 5 min in a microwave. After cooling, the sections were rinsed in TBS for 30 min.

2.4. Immunohistochemical analysis

Immunohistochemical analysis was performed in accordance with the standard ABC method. To reduce nonspecific staining, sections were treated with 5% bovine serum albumin (BSA) and 3% goat serum in TBS for 1 h. They were

then incubated with primary antibodies specific against ZnT1 and ZnT3–7 overnight at 4 °C. Antibodies were diluted in TBS containing 3% normal goat serum (NGS), 1% BSA, and 0.25% Triton X-100 at 1:50 for ZnT1, ZnT3, ZnT6 antibodies and at 1:25 for ZnT4, ZnT5, ZnT7 antibodies. After several rinses in TBS, the sections were incubated with a 1:200 diluted biotinylated goat anti-rabbit IgG for 1 h at room temperature. To visualize the immunoreaction sites in tissues, the sections were then rinsed and treated with reagents from an ABC Kit for 1 h at room temperature. The sections were rinsed in TBS and incubated with 0.025% 3,3-diaminobenzidine (DAB) plus 0.0033% H_2O_2 in TBS for 10 min. Then, Tris buffer was added to stop the DAB reaction. The stained sections were dehydrated through graded alcohols, cleared in xylene, and covered with neutral balsam. All sections were examined and images were taken with a light microscope equipped with a digital color camera. The images were further processed with Adobe Photoshop.

2.5. Immunofluorescence analysis

All immunofluorescence procedures were performed at room temperature. NDS, primary and secondary antibodies were all diluted in 0.01 M PBS containing 1% BSA and 0.25% Triton X-100.

For single labeling with Aβ, sections were preincubated with NDS (1:20) for 1 h and then incubated with mouse anti-Aβ (1:500) at room temperature overnight. After several rinses, the sections were incubated with Texas Red-conjugated donkey anti-mouse IgG (1:50) for 2 h. After rinsing with 0.01 M PBS, the sections were mounted with an anti-fading mounting medium and examined using a macro zoom fluorescence microscope (MVX10, Olympus). Images were taken using a microscope equipped with a digital color camera (DP71, Olympus).

For double labeling, sections were preincubated with NDS (1:20) for 1 h and then incubated overnight in a mixture of primary antibodies, mouse anti-Aβ (1:500) and rabbit anti-ZnT1 (1:50), ZnT3 (1:50) ZnT4 (1:25), ZnT5 (1:25), ZnT6 (1:50) or ZnT7 (1:25). After several rinses, the sections were incubated for 2 h with a mixture of secondary antibodies, FITC-conjugated donkey anti-rabbit IgG (1:50, for labeling one of the ZnTs) and Texas Red-conjugated donkey anti-mouse IgG (1:50, for labeling Aβ). After rinsing with PBS, the sections were mounted with an anti-fading mounting medium and examined using a confocal laser scanning microscope (SP2, Leica). Excitation filters for FITC (488 nm) and Texas-Red (568 nm) were used. Images were taken using Kalman mode scanning (10 scans) from single channel scanning. Colocalization was verified by a sequential scan between the two channels. Images were processed using an Adobe Photoshop program.

To assess nonspecific staining, a few sections in every experiment were incubated with NDS instead of primary antibodies followed by all subsequent incubations as described above.

2.6. Immersion autometallography

One- and two-millimeter-thick slices of brain tissues were cut with a "fast tissue slicer" (Histotech, Denmark) and immersed in NTS (0.1% sodium sulphide and 3% glutaraldehyde in 0.1 M phosphate buffer, pH 7.4). The immersion jars were placed on a shaker and kept at 4 °C. Three days later, the slices were carefully rinsed twice in a 0.1 M phosphate buffer for 10 min. For light microscopy, the brain slices were placed in a 30% sucrose solution until they sank to the bottom of the glass. They were then frozen with CO_2 and placed in a cryostat, and the temperature was lowered to −17 °C. After AMG development (see below), the sections were counterstained with a 0.1% aqueous toluidine blue (pH 4.0) solution, dehydrated in ascending concentrations of alcohol and xylene, embedded in DEPEX, and covered with a cover slide. They were then analyzed and photographed with a light microscope. For electron microscopy, vibratome sections were prepared and immersed in AMG developer. After AMG staining, the areas to be analyzed were cut out, placed in osmium tetroxide (1% in phosphate buffer for 30 min) and embedded in Epon. The ultrathin sections were cut, placed on a grid and counterstained with uranyl acetate and lead citrate (Danscher, 1981; Danscher et al., 2004; Danscher and Stoltenberg, 2006).

The AMG developer consisted of a 60 ml gum arabic solution, 10 ml sodium citrate buffer, 15 ml reducing agent (0.85 g hydroquinone in 15 ml distilled water at 40 °C), and 15 ml of a solution containing silver ions (0.12 g silver lactate in 15 ml distilled water at 40 °C, added immediately before use while thoroughly stirring the AMG solution). Glass slides were placed in Farmer cleaned jars filled with the AMG developer and incubated at 26 °C for 60 min while being gently shaken. The AMG development was stopped by replacing the developer with a 5% sodium thiosulphate solution (in distilled water) for 10 min (AMG stop bath). Jars were then placed under gently running deionized water for 5 min (Danscher, 1981; Danscher et al., 2004; Danscher and Stoltenberg, 2006). The entire set-up was prepared in

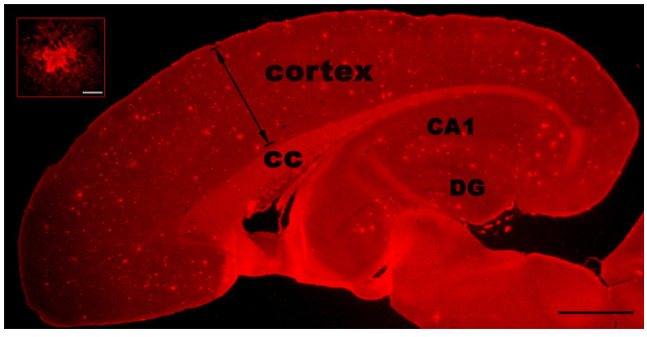

Fig. 1. Immunofluorescence staining of Aβ in the APP/PS1 transgenic mouse brain. The Aβ-positive senile plaques are widely distributed in almost all the cortical layers and the CA1 and dentate gyrus (DG) region of the hippocampus. cc, Corpus callosum. Scale bar = 2 mm. The insert is a higher magnification of an Aβ-positive senile plaque. Scale bar = 20 μm.

plain daylight on the lab bench. However, the development procedure was performed in darkness.

The mandatory DEDTC (sodium diethyldithiocarbamate trihydrate; Merck, 6689) control procedure was performed to ensure the specificity of the zinc ion staining (Danscher et al., 1973; Stoltenberg et al., 2005; Danscher and Stoltenberg, 2006).

2.7. Western blot analysis

The hippocampus and cortex of brains were homogenized at 1:5 (w:v) in an ice-cold lysis buffer (50 mM Tris–HCl, 150 mM NaCl, 1% Nonidet P-40, 1 mM EDTA, 0.25% sodium deoxicolate, 0.1% SDS, 1 mM phenylmethylsulfonyl fluoride (PMSF), 10 mg/ml leupeptin, 1 mM Na_3VO_4, and

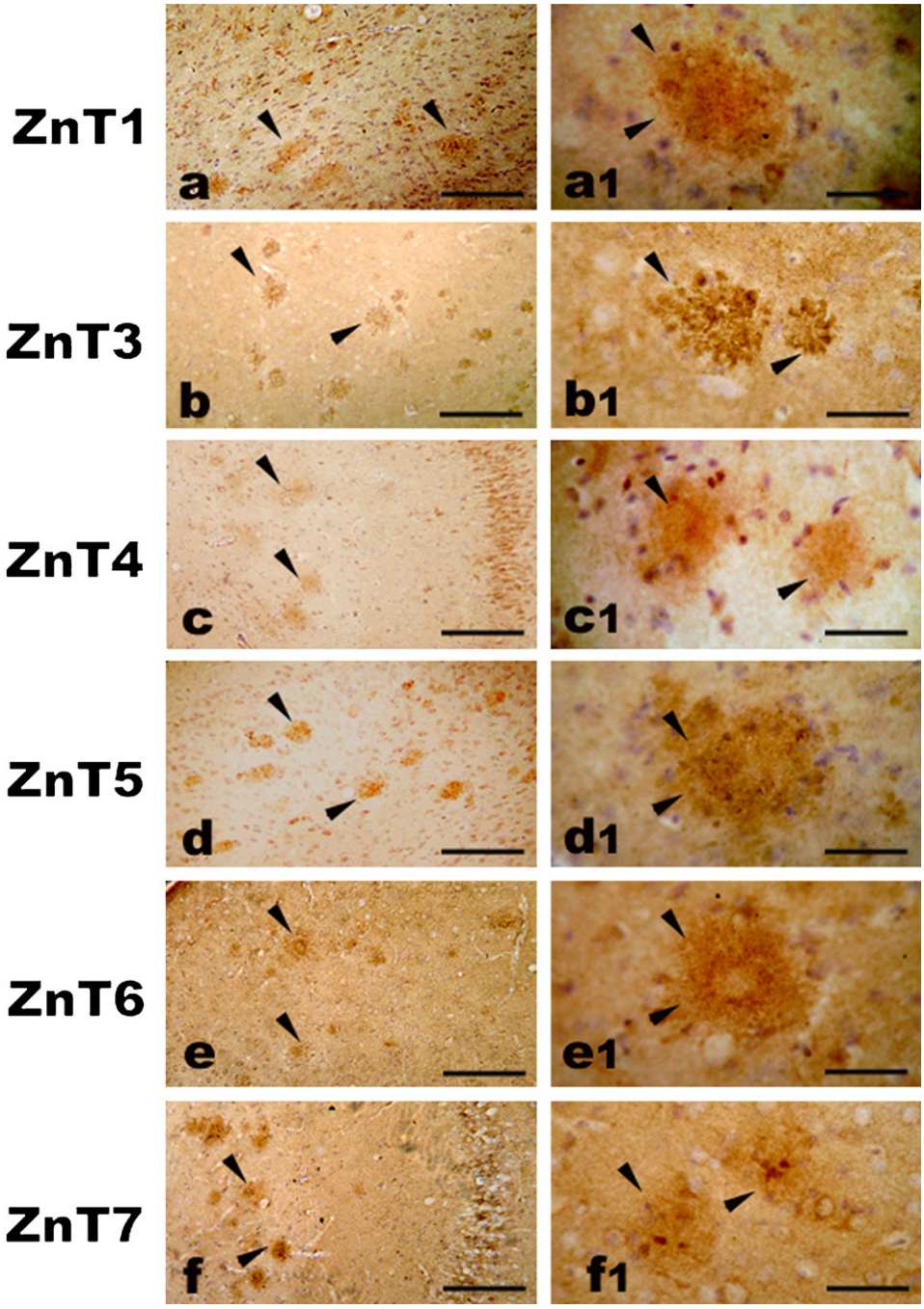

Fig. 2. Immunohistochemical analysis of ZnT1, ZnT3, ZnT4, ZnT5, ZnT6, and ZnT7 in the SP. Low magnification showing abundant expression of ZnTs in the SP (arrowheads in a–f). High magnification showing different staining patterns and intensities of ZnTs in the SP (a1–f1). Arrowheads indicate the staining of ZnT proteins. ZnT1 and ZnT4 are extensively expressed all over the plaques (arrowheads in a1 and c1), while ZnT3, ZnT5, and ZnT6 are prominently concentrated in the degenerating neurites in the periphery of the plaques (arrowheads in b1, d1, and e1). ZnT7 is present in all parts of the plaque, but is particularly dense in the centre of the plaque (arrowhead in f1). Scale bars = 100 μm (a–f); 10 μm (a1–f1).

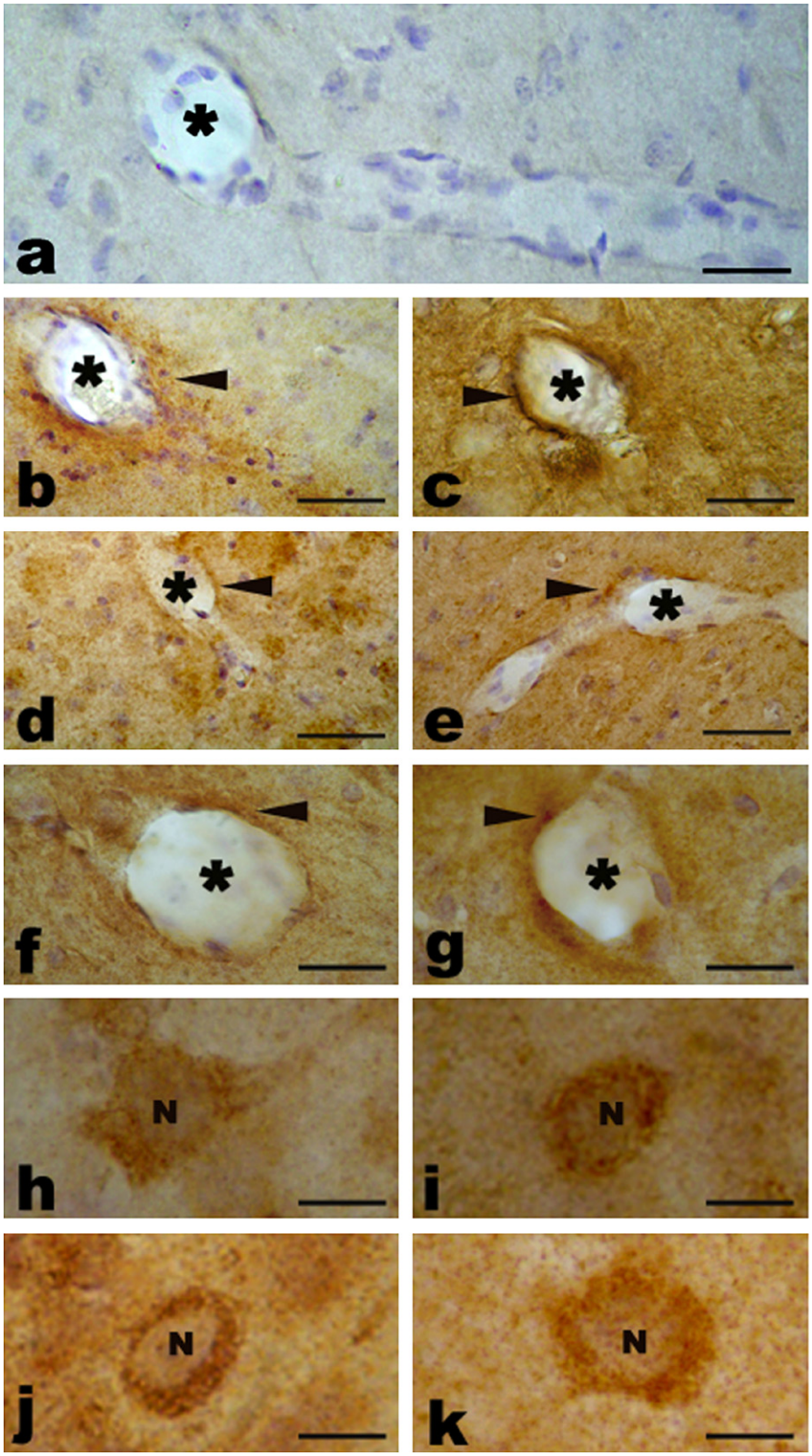

Fig. 3. Distribution of ZnT1, ZnT3, ZnT4, ZnT5, ZnT6, and ZnT7 in the cerebral blood vessels in the APP/PS1 transgenic mouse brain. Immunohistochemical staining shows that all members of ZnT family examined are expressed within the wall or in the vicinity of cerebral vessels (a, negative control; b, ZnT1, from cortex; c, ZnT3, from hippocampus; d, ZnT4, from cortex; e, ZnT5, from hippocampus; f, ZnT6, from hippocampus; g, ZnT7, from cortex). ZnT3 immunoreactivity is the most intense among the ZnTs examined (c). Asterisks (*) indicate the lumen of blood vessels. ZnT4 (h), ZnT5 (i), ZnT6 (j), and ZnT7 (k) are abundantly expressed in the neuronal cell bodies. N, nucleus. Scale bars = 50 μm (a–e); 20 μm (f–g); 10 μm (h–k).

1 mM NaF). The resulting homogenate was centrifuged at 12,000 × *g* for 30 min at 4 °C. The supernatant was collected and total protein levels were measured by a BCA protein assay kit (Pierce Biotechnology).

Proteins (20 μg) were separated on 10% SDS-polyacrylamide gels and transferred onto PVDF membranes (Millipore, CA) in an electronasfer device (45 V, 15 h). The membranes were blocked in 5% nonfat milk in TBS containing 0.05% Tween 20 (TTBS) for 3 h and then incubated with a primary antibody overnight at 4 °C. The dilutions of primary antibodies were 1:500 for ZnT1, ZnT3, ZnT4, ZnT6, and ZnT7, 1:1000 for ZnT5, and 1:12,000 for GAPDH. The membranes were washed with TTBS, incubated with a horseradish peroxidase-conjugated secondary antibody for 2 h at room temperature at constant stirring, washed and reacted with reagents in an enhanced chemiluminescence (ECL) kit (Pierce, CA). Protein bands were visualized by exposure to Kodak-XAR film. After development, the band intensities were quantified using an Image-pro Plus 6.0 analysis software.

Specificities of the antibodies against ZnT1 and ZnT3–7 were described previously by Western blot analyses (Palmiter et al., 1996b; Huang et al., 2002; Sekler et al., 2002; Kirschke and Huang, 2003; Yu et al., 2007).

2.8. Statistical analysis

Mean protein levels of ZnTs in APPswe/PS1dE9 transgenic mice and wild-type mice were compared using a two-tailed Student's *t*-test. Results are presented as mean ± S.E.M. (% of wild-type controls). $P < 0.05$ was considered significant.

3. Results

3.1. Aβ immunoreactivity showed extensive senile plaques in the APP/PS1 transgenic mouse cerebrum

Macro zoom fluorescence microscope analysis showed an overall immunofluorescence staining of Aβ in the cerebrum of the APP/PS1 transgenic mice (Fig. 1). The Aβ-positive senile plaques were widely distributed in the CA1 and dentate gyrus (DG) region of the hippocampus and almost all the cortical layers (Fig. 1). The plaques were different in sizes, textures, and immunofluorescence intensities. These results were consistent with previous reports that the APP/PS1 transgenic mouse brain, especially the hippocampus and cortex, contained a large amount of Aβ-positive plaques when animals were 6–7 months old (Flood et al., 2002; Van-Groen et al., 2006).

3.2. Abundant expression of ZnTs in SP and amyloid angiopathic vessels

Routine immunohistochemical observations revealed abundant expression of ZnTs in the amyloid plaques. Fig. 2 shows the overall immunohistochemical localization of ZnTs in the cerebrum of the APP/PS1 transgenic mice. In general, ZnTs-positive plaques were observed throughout the

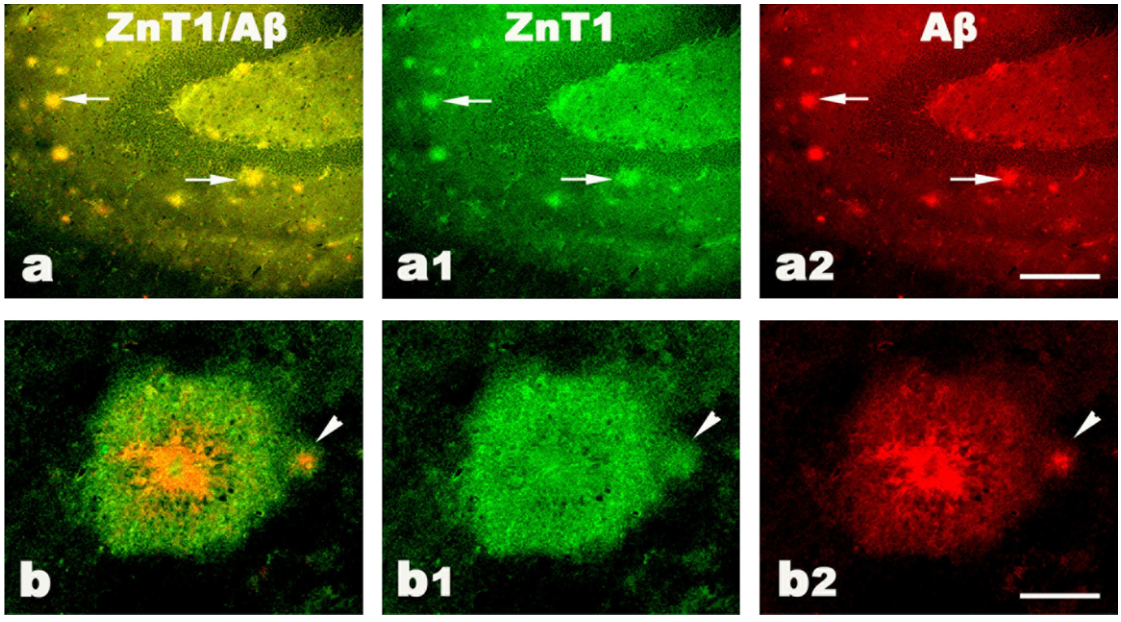

Fig. 4. Double-immunofluorescence labeling of ZnT1 and Aβ. Low magnification showing abundant expression of ZnT1 in the Aβ-positive plaques (a1 and a2). A colocalization of ZnT1 and Aβ is detected in most plaques (arrows in a). High magnification showing a large and a small plaque (arrowheads in b–b2). The two plaques are Aβ-positive and display typical characteristics of a cored plaque that contains a dense core of tightly aggregated amyloid fibrils and loosely arranged radially oriented amyloid fibrils (b2). ZnT1 is expressed all through the plaques (b1). Scale bars = 300 μm (a–a2); 30 μm (b–b2).

cortex and the CA1 and DG region of the hippocampus (Fig. 2a–f). At a higher magnification, ZnT1 (Fig. 2a1) and ZnT4 (Fig. 2c1) were extensively expressed in all parts of the plaques. ZnT3 (Fig. 2b1), ZnT5 (Fig. 2d1), and ZnT6 (Fig. 2e1) were expressed prominently in the degenerating neurites in the peripheral part of the plaques, while ZnT7 (Fig. 2f1) was present in the core of the plaques.

Our data also showed an abundant expression of ZnTs in the amyloid angiopathic vessels (Fig. 3). ZnT3 immunoreactivity was the most intense (Figs. 3c and 5c, c1). ZnT1 and ZnT4–7, were also expressed within the wall or in the vicinity of cerebral vessels (Fig. 3b, d–g), but far less than ZnT3. Furthermore, ZnT4–7 were all expressed in the neuronal cell bodies (Fig. 3h–k), in agreement with previous findings (Wenzel et al., 1997; Huang and Gitschier, 1997; Huang et al., 2002; Kirschke and Huang, 2003).

No distinct staining was observed in the negative control for the immunohistochemical staining in the brain tissue of APPswe/PS1dE9 transgenic mouse (Fig. 3a).

Double-immunofluorescence staining for Aβ and one of the zinc transporter proteins including ZnT1 and ZnT3–7 were performed to analyze the colocalization of Aβ and ZnT protein expression in the brains of APP/PS1 transgenic mice. As shown in Figs. 4–9, panel a1, expression of ZnTs was detected in the SP. Merging of ZnTs- and Aβ-labeled images from the two channels indicated that ZnT1 and ZnT3–7 were expressed in most of the Aβ containing plaques (Figs. 4–9, panels a and a2). At higher magnification, the majority of Aβ containing plaques showed a typical characteristic of senile plaques, such as a dense core of tightly aggregated amyloid fibrils surrounded by more radially oriented amyloid fibrils (Figs. 4–7, panel b2). Compact plaques containing densely packed Aβ fibrils throughout the plaques were also seen (Figs. 8 and 9, panel b2). ZnTs, however, exhibited different staining patterns. ZnT1 and ZnT4 were expressed all over the plaques (Figs. 4 and 6, panel b1), while ZnT3, ZnT5, and ZnT6 were concentrated primarily in the degenerating neurites in the periphery of the plaques (Figs. 5, 7 and 8, panel

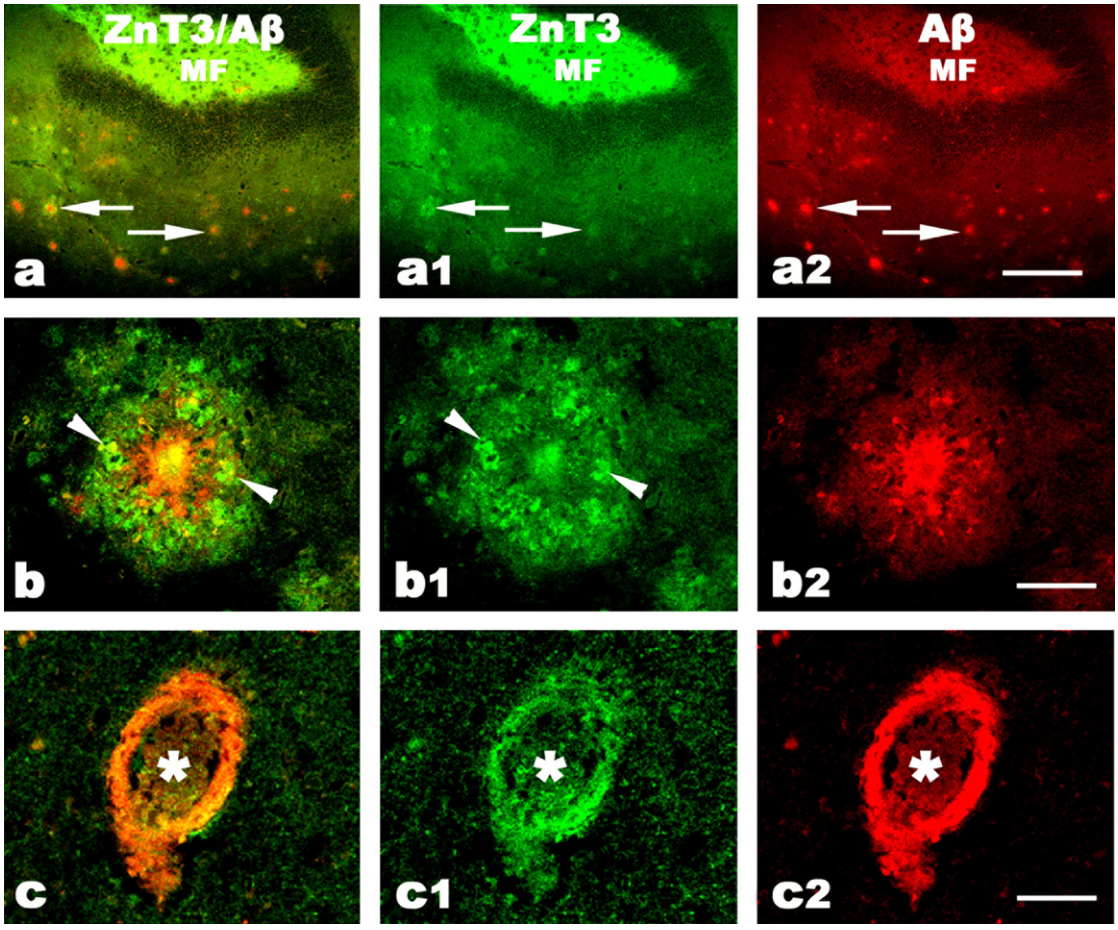

Fig. 5. Double-immunofluorescence labeling of ZnT3 and Aβ. Low magnification demonstrating abundant expression of ZnT3 in the Aβ-positive plaques (a1 and a2). An overlapping staining between ZnT3 and Aβ is seen in most plaques (arrows in a). An intense ZnT3 fluorescence is also seen in the hippocampal mossy fiber. High magnification showing a large Aβ-positive cored plaque (b2). ZnT3 is prominently concentrated in the degenerating neurites in the periphery of the plaque (b and b1, arrowheads indicated ZnT3 immunoreactivity). High magnification also shows the strongest ZnT3 immunoreactivity in the amyloid angiopathic vessel (c–c2). MF, mossy fiber. Asterisks (*) indicate the lumen of blood vessels. Scale bars = 300 μm (a–a2); 30 μm (b–b2 and c–c2).

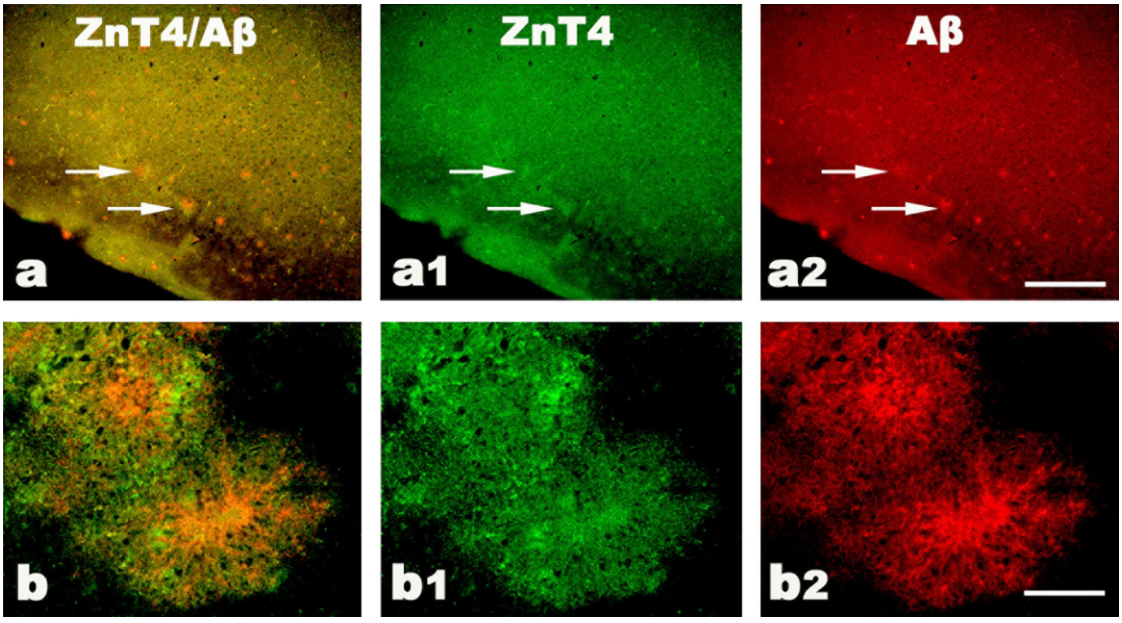

Fig. 6. Double-immunofluorescence labeling of ZnT4 and Aβ. Low magnification demonstrating co-expression between ZnT4 and Aβ in most plaques (arrows in a–a2). High magnification showing abundant expression of ZnT4 ((b and b1) in all parts of two amyloid plaques (b and b2)). Scale bars = 300 μm (a–a2); 30 μm (b–b2).

b1). In addition, ZnT5 and ZnT6 were completely absent from the center of the plaques (Figs. 7 and 8, panel b1). ZnT7 was present in all parts of the plaques, but particularly dense in the center of the plaques (Fig. 9b1). An intense ZnT3 fluorescence was seen in the hippocampal mossy fibers (Fig. 5a and a1).

3.3. Distribution of zinc ions in the senile plaques

Immersion autometallography is a highly sensitive method to trace free zinc ions in tissues (Danscher et al., 2004). We used this method to determine the distribution of free zinc ions in the senile plaques. Light microscopic observations showed

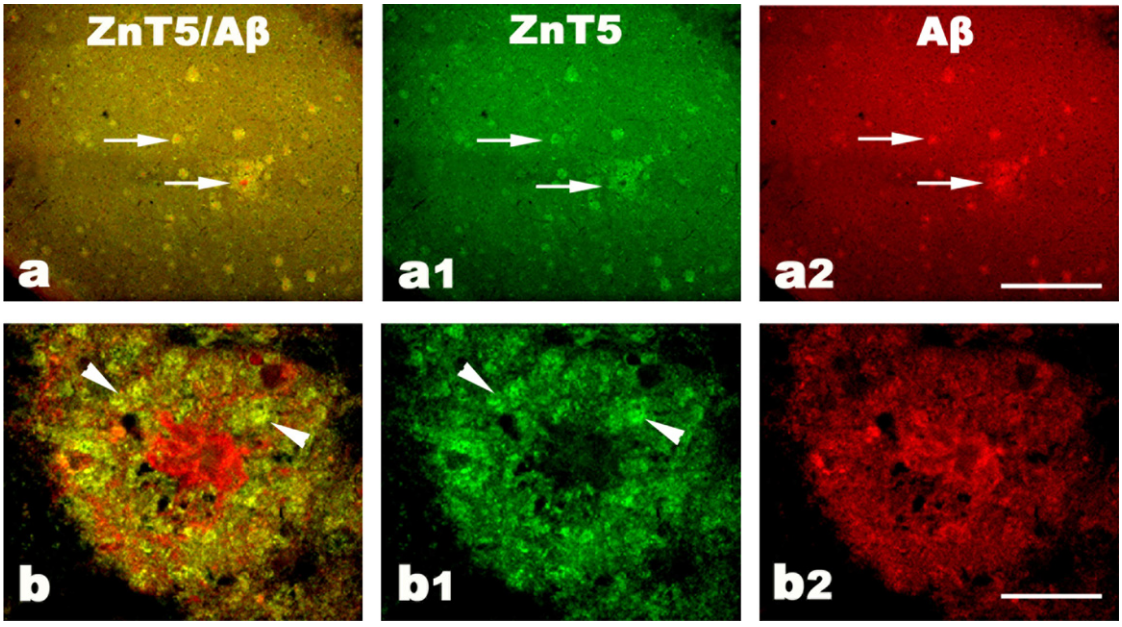

Fig. 7. Double-immunofluorescence labeling of ZnT5 and Aβ. Low magnification showing that almost all Aβ-positive plaques are ZnT5-positive (arrows in a–a2). High magnification showing a large Aβ-positive cored plaque (b2). ZnT5 is absent from the center and prominently concentrated in the degenerating neurites in the periphery region of the plaque (arrowheads in b and b1). Scale bars = 300 μm (a–a2); 30 μm (b–b2).

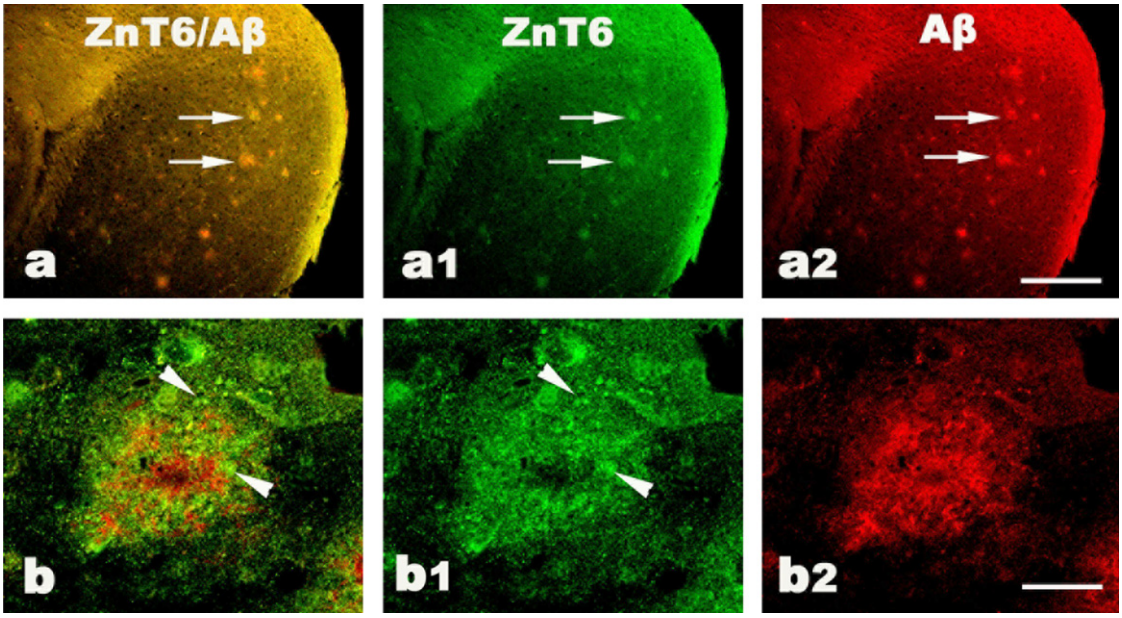

Fig. 8. Double-immunofluorescence labeling of ZnT6 and Aβ. Low magnification demonstrating abundant expression of ZnT6 and Aβ in the amyloid plaques (arrows in a–a2). High magnification showing a large Aβ-positive compact plaque containing densely packed Aβ fibrils in whole plaque (b2). ZnT6 is absent from the centre and prominently concentrated in the degenerating neurites in the periphery region of the plaque (arrowheads in b and b1). Scale bars = 300 μm (a–a2); 30 μm (b–b2).

that AMG-positive plaques were widely distributed in the APPswe/PS1dE9 transgenic mouse brain. The diameters of the plaques were approximately 10–100 μM (Fig. 10a). AMG-positive cerebral blood vessels can be seen clearly indicating the abundant distribution of zinc ions in the blood vessels wall (Fig. 10b). At higher magnification, a majority of the AMG-stained plaques were rosette-shaped with a non-zinc stained interior (Fig. 10c). Furthermore, electron microscopic analysis of plaques confirmed that the amyloid deposits were surrounded by neurites, and the distinct zinc staining could be seen clearly in the amyloid core (Fig. 10d) and the surrounding dystrophic neurites (Fig. 10e), in agreement with previous reports (Kurt et al., 2001; Boutajangout et al., 2004; Stoltenberg et al., 2007)

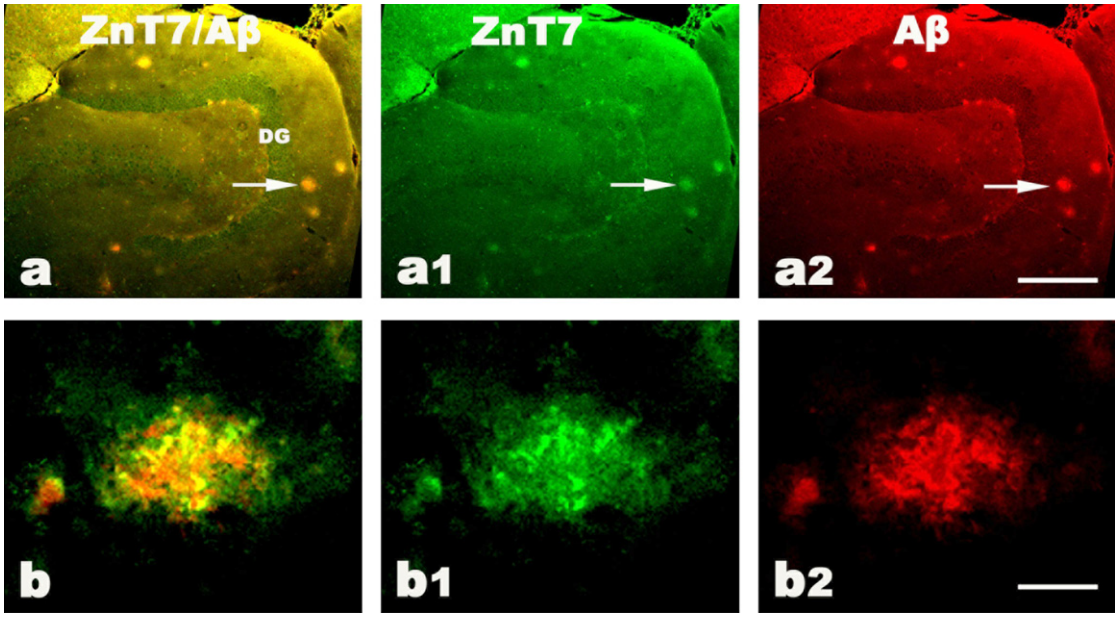

Fig. 9. Double-immunofluorescence labeling of ZnT7 and Aβ. Low magnification showing abundant expression of ZnT7 in the Aβ-positive plaques (a1 and a2). A colocalization of ZnT7 and Aβ is seen in most plaques (arrow in a). High magnification showing a medium-sized compact plaque containing densely packed Aβ fibrils in the whole plaque (b2). ZnT7 is expressed in the whole plaque, especially in the center of the plaque (b and b1). Scale bars = 300 μm (a–a2); 30 μm (b–b2).

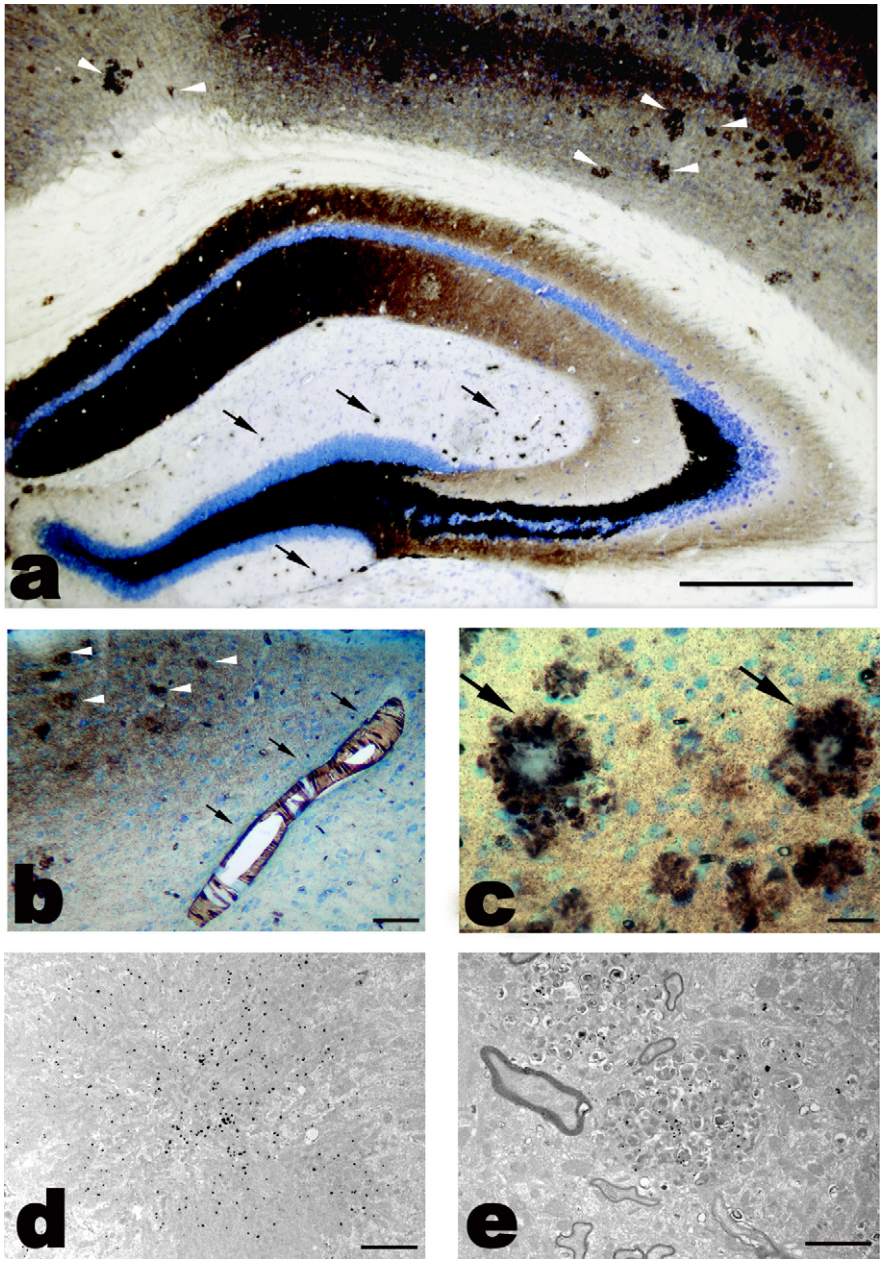

Fig. 10. Light micrographs (a–c) and electron micrographs (d and e) of AMG staining of zinc ions within the cortex and hippocampus of APP/PS1 transgenic mouse brain. Groups of zinc-stained plaques are shown by arrows within the hippocampus and by arrowheads within the cortex (a). Distinct zinc staining in the blood vessel wall (b). High magnification showing most of the zinc-stained plaques are rosette-shaped with a non-zinc stained core (c). Electron micrograph showing distinct zinc staining in an amyloid core of a plaque (d) and dystrophic neuritis (e). Scale bars = 500 μm (a); 100 μm (b); 10 μm (c); 3 μm (d); 2 μm (e).

3.4. Increased expression of ZnTs in the hippocampus and cortex

The levels of zinc transporter protein expression in the hippocampus and cortex were measured using Western blot analysis (Figs. 11 and 12). Our Western blot results indicated that the expression of zinc transporter proteins was increased in the hippocampus and cortex of APPswe/PS1dE9 transgenic mice. Among the zinc transporter proteins examined, ZnT3 showed the greatest increase in both hippocampus and cortex (398.6 ± 13.1% and 201.9 ± 11.4%, respectively, $P < 0.05$). ZnT6 and ZnT7 showed the smallest increase in hippocampus and cortex, respectively (142.2 ± 14.2% and 122.9 ± 2.8%, respectively, $P < 0.05$) (Figs. 11 and 12). Although the expression of ZnT5 was increased in the hippocampus and cortex of APPswe/PS1dE9 mice (168.2 ± 16.4% and 134.2 ± 9.0%, respectively), the changes were not statistically significant ($P < 0.1$) (Figs. 11 and 12).

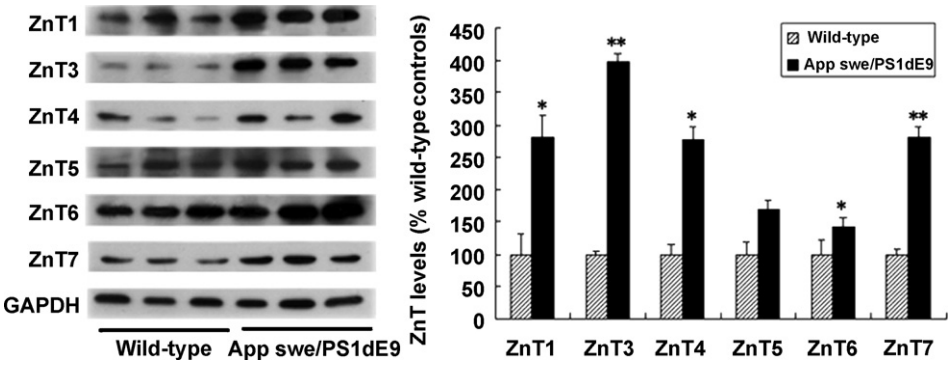

Fig. 11. Zinc transporter proteins expression in the hippocampus of APP/PS1 transgenic mice and wild-type controls. GAPDH was used as a control for protein loading. Results are presented as mean ± S.E.M. (% of wild-type controls), $n = 6$. $^{**}P < 0.01$ (vs. wild-type controls), $^{*}P < 0.05$ (vs. wild-type controls).

4. Discussion

Significant elevations and redistribution of zinc ions have been found in the human AD brain (Samudralwar et al., 1995; Deibel et al., 1996; Danscher et al., 1997; Lovell et al., 1998; Stoltenberg et al., 2005; Miller et al., 2006; Religa et al., 2006) and in the APP transgenic mouse brain (Tg2576) (Lee et al., 1999; Friedlich et al., 2004). In the present study, the distribution of zinc ions and six members of the ZnT family, ZnT1 and ZnT3–7, were investigated in the hippocampus and cortical layers of the APPswe/PS1dE9 transgenic mouse brain. Our current findings of the enrichment of zinc ions and co-expression of zinc transporter proteins with Aβ in amyloid plaques in the APPswe/PS1dE9 double mutant mouse brain extended the previous findings and demonstrated that zinc is an important component of senile plaques in both humans and mutant transgenic mice.

Previous studies from our laboratory and others have demonstrated that the zinc transporter proteins have different cellular and subcellular locations and play different roles in zinc homeostasis in normal and pathological conditions (Cousins and McMahon, 2000; Wang et al., 2002, 2003, 2004, 2005; Kambe et al., 2004). ZnT1, an ubiquitous zinc transporter localized on the plasma membrane, serves an essential function of zinc efflux from the cell (Palmiter and Findley, 1995; Nitzan et al., 2002; Sekler et al., 2002; Andrews et al., 2004), while other ZnTs are localized on the intracellular membranes and involved in pumping zinc into different intracellular organelles when cellular zinc levels are elevated (Kambe et al., 2004). Exposure to a high dose of zinc can induce an up-regulation of the ZnT1 gene in cultured cells (Langmade et al., 2000; Tsuda et al., 1997). Therefore, we hypothesize that the increased expression of ZnT1 and subsequent efflux of zinc ions cause an elevation of zinc ions in the extracellular space, which might initiate the increased deposition of Aβ and result in the creation of β-amyloid plaque. Furthermore, the high level of extracellular zinc ion, in turn, might up-regulate the expression of ZnT1. ZnT3 is mainly localized in the membranes of zinc-rich synaptic vesicles within mossy fiber buttons of hippocampus (Wenzel et al., 1997). Synaptic zinc release causes Aβ to precipitate into amyloid (Bush et al., 1994a; Huang et al., 1997; Lee et al., 2002; Friedlich et al., 2004). ZnT3 knockout mice are devoid of zinc ions in zinc-enriched terminals (Cole et al., 1999). Genetic ablation of ZnT3 in the Tg2576 Alzheimer mouse model inhibits amyloid pathology (Lee et al., 2002; Friedlich et al., 2004). Aβ accumulation has been reported in the endosomal/lysosomal system in postmortem AD brains (Takahashi et al., 2002) and precedes amyloid plaque formation (Wirths et al., 2001; Shie et al., 2003). ZnT4 may have a role in this process as it is localized on the intracellular vesicular membrane and functions to increase vesicular zinc

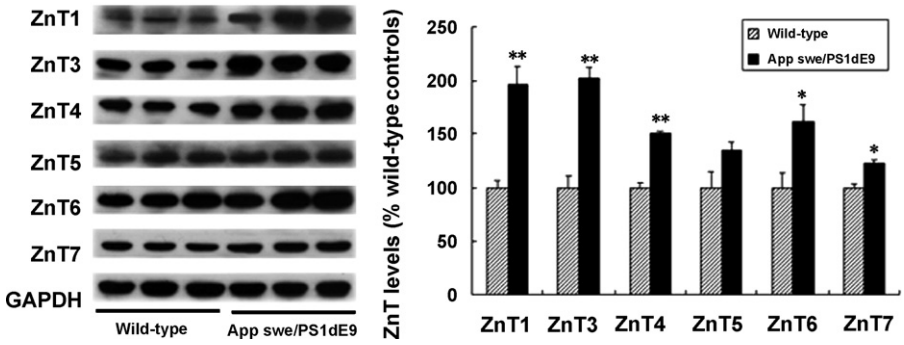

Fig. 12. Zinc transporter proteins expression in the neo-cortex of APP/PS1 transgenic mice and the wild-type controls. GAPDH was used as a control for protein loading. Results are presented as mean ± S.E.M. (% of wild-type controls), $n = 6$. $^{**}P < 0.01$ (vs. wild-type controls), $^{*}P < 0.05$ (vs. wild-type controls).

concentration. The functions of ZnT5, ZnT6, and ZnT7 are believed to facilitate the translocation of the cytoplasmic zinc into the Golgi apparatus (Huang et al., 2002; Kirschke and Huang, 2003; Chi et al., 2006). Interestingly, the γ-secretase complex responsible for the cleavage of APP interacts with its substrates in the trans-Golgi network (TGN) (Baulac et al., 2003). There are different Aβ compositions in different portions of one plaque or different plaque types (Güntert et al., 2006; Harigaya et al., 2006). Our findings of complex zinc transporter expression patterns in the plaques and the elevated expression of ZnTs in the hippocampus and cortex of the APPswe/PS1dE9 transgenic mice suggest that zinc transporters may play multiple roles in the deposition and organization of Aβ composition.

For the first time, Friedlich et al. (2004) reported the contribution of zinc to vascular β-amyloid deposition in APP transgenic mice brain. It has been suggested that the amount of zinc in the CAA is dependent on ZnT3 activity as the amount of CAA and zinc levels in the cerebral vessel walls are decreased in $APP^{+}/ZnT3^{+/-}$ and $APP^{+}/ZnT3^{-/-}$ mice. However, the amount of CAA of $APP^{+}/ZnT3^{-/-}$ mice increases when the mice are 15–18 months old, indicating apart from ZnT3, there is another source of zinc ions that contributes to CAA formation. Our results showed that together with the strong expression of ZnT3 in the wall and the vicinity of CAA changed vessels, other ZnTs are also moderately or faintly expressed in the same regions. We therefore hypothesize that, apart from the significant functions of ZnT3, the elevated zinc ions that initiate the amyloid precipitation in the formation of the CAA pathology in the aging mice may be also associated with the abnormal activities of other members of the ZnT family.

In summary, the present study provided morphological evidence of ZnTs being involved in the formation of SPs and CAAs in APPswe/PS1dE9 transgenic mice. Although the patterns and levels of zinc transporter protein expression differed somewhat among the different transporters, their expression was increased in the brain of APPswe/PS1dE9 transgenic mice. Furthermore, their expression was more abundant in the plaques and CAA changed vessels than in the surrounding tissue, suggesting that ZnTs may play significant roles in the deposition of Aβ.

Disclosure statement

We state that there are no potential conflicts of interest, including any financial, personal or other relationships with people or organizations that could inappropriatedly influence the current study.

Acknowledgements

The study was supported by Natural Science Foundation of China (30770680, 30670722, 30370452), Program for New Century Excellent Talents in University (NCET-04-0288), China Postdoctoral Science Foundation (2005037008), Specialized Research Fund for the Doctoral Program of Higher Education (SRFDP-20060159001), the United States Department of Agriculture (CRIS-5603-515-30-014-00D), and The Lundbeck Foundation of Denmark.

References

Andrews, G.K., Wang, H.B., Dey, S.K., Palmiter, R.D., 2004. Mouse zinc transporter 1 gene provides an essential function during early embryonic development. Genesis 40, 74–81.

Baulac, S., LaVoie, M.J., Kimberly, W.T., Strahle, J., Wolfe, M.S., Selkoe, D.J., Xia, W., 2003. Functional-secretase complex assembly in Golgi/trans-Golgi network: interactions among presenilin, nicastrin, Aph1, Pen-2,-secretase substrates. Neurobiol. Dis. 14, 194–204.

Boutajangout, A., Authelet, M., Blanchard, V., Touchet, N., Tremp, G., Pradier, L., Brion, J.P., 2004. Characterisation of cytoskeletal abnormalities in mice transgenic for wild-type human tau and familial Alzheimer's disease mutants of APP and presenilin-1. Neurobiol. Dis. 15, 47–60.

Bush, A.I., 2002. Metal complexing agents as therapies for Alzheimer's disease. Neurobiol. Aging 6, 1031–1038.

Bush, A.I., Pettingell, W.H., Multhaup, G., Paradis, M.D., Vonsattel, J.P., Gusella, J.F., Beyreuther, K., Masters, C.L., Tanzi, R.E., 1994a. Rapid induction of Alzheimer A beta amyloid formation by zinc. Science 265, 1464–1467.

Bush, A.I., Pettingell, W.H., Paradis, M.D., Tanzi, R.E., 1994b. Modulation of A beta adhesiveness and secretase site cleavage by zinc. J. Biol. Chem. 269, 12152–12158.

Cherny, R.A., Atwood, C.S., Xilinas, M.E., Gray, D.N., Jones, W.D., McLean, C.A., Barnham, K.J., Volitakis, I., Fraser, F.W., Kim, Y., Huang, X., Goldstein, L.E., Moir, R.D., Lim, J.T., Beyreuther, K., Zheng, H., Tanzi, R.E., Masters, C.L., Bush, A.I., 2001. Treatment with a copper-zinc chelator markedly and rapidly inhibits betaamyloid accumulation in Alzheimer's disease transgenic mice. Neuron 30, 665–676.

Chi, Z.H., Wang, X., Wang, Z.Y., Gao, H.L., Dahlstrom, A., Huang, L.P., 2006. Zinc transporter 7 is located in the cis-Golgi apparatus of mouse choroid epithelial cells. Neuroreport 17, 1807–1811.

Christianson, D.W., 1991. Structural biology of zinc. Adv. Protein Chem. 42, 281–355.

Cole, T.B., Wenzel, H.J., Kafer, K.E., Schwartzkroin, P.A., Palmiter, R.D., 1999. Elimination of zinc from synaptic vesicles in the intact mouse brain by disruption of the ZnT3 gene. Proc. Natl. Acad. Sci. U.S.A. 96, 1716–1721.

Coleman, J.E., 1992. Zinc proteins: enzymes, storage proteins, transcription factors, and replication proteins. Annu. Rev. Biochem. 61, 897–946.

Colvin, R.A., Fontaine, C.P., Laskowski, M., Thomas, D., 2003. Zn^{2+} transporters and Zn^{2+} homeostasis in neurons. Eur. J. Pharmacol. 479, 171–185.

Cousins, R.J., McMahon, R.J., 2000. Integrative aspects of zinc transporters. J. Nutr. 130, 1384–1387.

Danscher, G., 1981. Histochemical demonstration of heavy metals. A revised version of the sulphide silver method suitable for both light and electron-microscopy. Histochemistry 71, 1–16.

Danscher, G., Stoltenberg, M., 2006. Silver enhancement of quantum dots resulting from (1) metabolism of toxic metals in animals and humans, (2) in vivo, in vitro and immersion created zinc-sulphur/zinc-selenium nanocrystals, (3) metal ions liberated from metal implants and particles. Prog. Histochem. Cytochem. 41, 57–139.

Danscher, G., Haug, F.M., Fredens, K., 1973. Effect of diethyldithiocarbamate (DEDTC) on sulphide silver stained boutons. Reversible blocking of Timm's sulphide silver stain for "heavy" metals in DEDTC treated rats (light microscopy). Exp. Brain Res. 16, 521–532.

Danscher, G., Jensen, K.B., Frederickson, C.J., Kemp, K., Andreasen, A., Juhl, S., Stoltenberg, M., Ravid, R., 1997. Increased amount of zinc in the hippocampus and amygdala of Alzheimer's diseased brains: a proton-induced X-ray emission spectroscopic analysis of cryostat sections from autopsy material. J. Neurosci. Methods 76, 53–59.

Danscher, G., Stoltenberg, M., Bruhn, M., 2004. Immersion autometallography: histochemical in situ capturing of zinc ions in catalytic zinc-sulfur nanocrystals. J. Histochem. Cytochem. 12, 1619–1625.

Deibel, M.A., Ehmann, W.D., Markesbery, W.R., 1996. Copper, iron, and zinc imbalances in severely degenerated brain regions in Alzheimer's disease: possible relation to oxidative stress. J. Neurol. Sci. 143, 137–142.

Eide, D.J., 2004. The SLC39 family of metal ion transporters. Pflugers Arch. 447, 796–800.

Fabrice, C., Severine, D., Alain, F., Michel, S., 2004. Identification and cloning of a cell specific zinc transporter, ZnT-8, localized into insulin secretory granules. Diabetes 53, 2330–2337.

Flood, D.G., Reaume, A.G., Dorfman, K.S., Lin, V.G., Lang, D.M., Trusko, S.P., Savage, M.J., Annaert, W.G., De-Strooper, B., Siman, R., Scott, R.W., 2002. FAD mutant PS-1 gene-targeted mice: increased A bata 42 and A bata deposition without APP overproduction. Neurobiol. Aging 23, 335–348.

Frederickson, C.J., Kasarskis, E.J., Ringo, D., Frederickson, R.E., 1987. A quinoline fluorescence method for visualizing and assaying the histochemically reactive zinc (bouton zinc) in the brain. J. Neurosci. Methods 20, 91–103.

Friedlich, A.L., Lee, J.Y., Groen, T.V., Cherny, R.A., Volitakis, I., Cole, T.B., Palmiter, R.D., Koh, J.Y., Bush, A.I., 2004. Neuronal zinc exchange with the blood vessel wall promotes cerebral amyloid angiopathy in an animal model of Alzheimer's disease. J. Neurosci. 24, 3453–3459.

Güntert, A., Dobeli, H., Bohrmann, B., 2006. High sensitivity analysis of amyloid-beta peptide composition in amyloid deposits from human and PS2/APP mouse brain. Neuroscience 143, 461–475.

Harigaya, Y., Tomidokoro, Y., Ikeda, M., Sasaki, A., Kawarabayashi, T., Matsubara, E., Kanai, M., Saido, T.C., Younkin, S.G., Shoji, M., 2006. Type-specific evolution of amyloid plaque and angiopathy in APPsw mice. Neurosci. Lett. 395, 37–41.

Huang, L., Gitschier, J., 1997. A novel gene involved in zinc transport is deficient in the lethal milk mouse. Nat. Genet. 17, 292–297.

Huang, X., Atwood, C.S., Moir, R.D., Hartshorn, M.A., Vonsattel, J.P., Tanzi, R.E., Bush, A.I., 1997. Zinc-induced Alzheimer's Abeta1-40 aggregation is mediated by conformational factors. J. Biol. Chem. 272, 26464–26470.

Huang, L., Kirschke, C.P., Gitschier, J., 2002. Functional characterization of a novel mammalian zinc transporter ZnT6. J. Biol. Chem. 277, 26389–26395.

Kambe, T., Yamaguchi-Iwai, Y., Sasakib, R., Nagao, M., 2004. Overview of mammalian zinc transporters. Cell Mol. Life Sci. 61, 49–68.

Kar, S., Slowikowski, S., Westaway, D., Mount, H., 2004. Interactions between beta-amyloid and central cholinergic neurons: implications for Alzheimer's disease. J. Psychiatr. Neurosci. 6, 427–441.

Kirschke, C.P., Huang, L., 2003. ZnT7, A novel mammalian zinc transporter, accumulates zinc in the Golgi apparatus. J. Biol. Chem. 278, 4096–4102.

Kurt, M.A., Davies, D.C., Kidd, M., Duff, K., Rolph, S.C., Jennings, K.H., Howlett, D.R., 2001. Neurodegenerative changes associated with beta-amyloid deposition in the brains of mice carrying mutant amyloid precursor protein and mutant presenilin-1 transgenes. Exp. Neurol. 171, 59–71.

Langmade, S.J., Ravindra, R., Daniels, P.J., Andrews, G.K., 2000. The transcription factor MTF-1 mediates metal regulation of the mouse ZnT1 gene. J. Biol. Chem. 275, 34803–34809.

Lee, J.Y., Mook, J.I., Koh, J.Y., 1999. Histochemically reactive zinc in plaques of the Swedish mutant beta-amyloid precursor protein transgenic mice. J. Neurosci. 19 (RC10), 1–5.

Lee, J.Y., Cole, T.B., Palmiter, R.D., Sang, W.S., Jae, Y.K., 2002. Contribution by synaptic zinc to the gender-disparate plaque formation in human Swedish mutant APP transgenic mice. Proc. Natl. Acad. Sci. U.S.A. 11, 7705–7710.

Lee, J.Y., Friedman, J.E., Angel, I., Kozak, A., Koh, J.Y., 2004. The lipophilic metal chelator DP-109 reduces amyloid pathology in brains of human beta-amyloid precursor protein transgenic mice. Neurobiol. Aging 25, 1315–1321.

Lovell, M.A., Robertson, J.D., Teesdale, W.J., Campbell, J.L., Markesbery, W.R., 1998. Copper, iron and zinc in Alzheimer's disease senile plaques. J. Neurol. Sci. 158, 47–52.

Lovell, M.A., Smith, J.L., Xiong, S.L., Markesbery, W.R., 2005. Alterations in zinc transporter protein-1 (ZnT-1) in the brain of subjects with mild cognitive impairment, early, and late- stage Alzheimer's disease. Neurotox. Res. 7, 265–271.

Mancini, M., Ricci, A., Amenta, F., 1992. Age-related changes in sulfide-silver staining in the rat neostriztum: a quantitative histochemical study. Neurobiol. Aging 13, 501–504.

Miller, L.M., Wang, Q., Telivala, T.P., Smith, R.J., Lanzirotti, A., Miklossy, J., 2006. Synchrotron-based infrared and X-ray imaging shows focalized accumulation of Cu and Zn co-localized with beta-amyloid deposits in Alzheimer's disease. J. Struct. Biol. 155, 30–37.

Miro-Bernie, N., Sancho-Bielsa, F.J., Lopez-Garcia, C., Perez-Clausell, J., 2003. Retrograde transport of sodium selenite and intracellular injection of micro-ruby: a combined method to describe the morphology of zinc-rich neurons. J. Neurosci. Methods 127, 199–209.

Nitzan, Y.B., Sekler, I., Hershfinkel, M., Moran, A., Silverman, W.F., 2002. Postnatal regulation of ZnT-1 expression in the mouse brain. Brain Res. 137, 149–157.

Palmiter, R.D., Findley, S.D., 1995. Cloning and characterization of a mammalian zinc transporter that confers resistance to zinc. EMBO J. 14, 639–664.

Palmiter, R.D., Huang, L., 2004. Efflux and compartmentalization of zinc by members of the SLC30 family of solute carriers. Pflugers Arch. 447, 744–751.

Palmiter, R.D., Cole, T.B., Findley, S.D., 1996a. ZnT-2 a mammalian protein that confers resistance to zinc by facilitating vesicular sequestration. EMBO J. 15, 1784–1791.

Palmiter, R.D., Cole, T.B., Quaife, C.J., Findley, S.D., 1996b. ZnT-3, a putative transporter of zinc into synaptic vesicles. Proc. Natl. Acad. Sci. U.S.A. 93, 14934–14939.

Pérez-Clausell, J., 1996. Distribution of terminal fields stained for zinc in the neocortex of the rat. J. Chem. Neuroanat. 11, 99–111.

Religa, D., Strozyk, D., Cherny, R.A., Volitakis, I., Haroutunian, V., Winblad, B., Naslund, J., Bush, A.I., 2006. Elevated cortical zinc in Alzheimer disease. Neurology 67, 69–75.

Samudralwar, D.L., Diprete, C.C., Ni, B.F., Ehmann, W.D., Markesbery, W.R., 1995. Elemental imbalances in the olfactory pathway in Alzheimer's disease. J. Neurol. Sci. 130, 139–145.

Sekler, I., Moran, A., Hershfinkel, M., Dori, A., Margulis, A., Birenzweig, N., Nitzan, Y., Silverman, W.F., 2002. Distribution of the zinc transporter ZnT-1 in comparison with chelatable zinc in the mouse brain. J. Comp. Neurol. 447, 201–209.

Seve, M., Chimienti, F., Devergnas, S., Favier, A., 2004. In silico identification and expression of SLC30 family genes: an expressed sequence tag data mining strategy for the characterization of zinc transporters' tissue expression. BMC Genomics 5, 32.

Shie, F.S., Le-Boeuf, R.C., Jin, L.W., 2003. Early intraneuronal Abeta deposition in the hippocampus of APP transgenic mice. Neuroreport 14, 123–129.

Sim, D.L., Chow, V.T., 1999. The novel human HUEL (C4 or f1) gene maps to chromosome 4p12-p13 and encodes a nuclear protein containing the nuclear receptor interaction motif. Genomics 59, 224–233.

Smith, J.L., Xiong, S., Markesbery, W.R., Lovell, M.A., 2006. Altered expression of zinc transporters-4 and -6 in mild cognitive impairment, early and late Alzheimer's disease brain. Neuroscience 140, 879–888.

Stoltenberg, M., Bruhn, M., Sondergaard, C., Doering, P., West, M.J., Larsen, A., Troncoso, J.C., Danscher, G., 2005. Immersion autometallographic tracing of zinc ions in Alzheimer beta amyloid plaques. Histochem. Cell Biol. 123, 605–611.

Stoltenberg, M., Bush, A.I., Bach, G., Smidt, K., Larsen, A., Rungby, J., Lund, S., Doering, P., Danscher, G., 2007. Amyloid plaques arise from zinc-enriched cortical layers in APP/PS1 transgenic mice and are paradoxically enlarged with dietary zinc deficiency. Neuroscience 150, 357–369.

Takahashi, R.H., Milner, T.A., Li, F., Nam, E.E., Edgar, M.A., Yamaguchi, H., Beal, M.F., Xu, H., Greengard, P., Gouras, G.K., 2002. Intraneuronal Alzheimer Abeta42 accumulates in multivesicular bodies and is associated with synaptic pathology. Am. J. Pathol. 161, 1869–1879.

Takeda, A., 2000a. Movement of zinc and its functional significance in the brain. Brain Res. Rev. 34, 137–148.

Takeda, A., 2001. Zinc homeostasis and functions of zinc in the brain. Bio Met. 14, 343–352.

Takeda, A., Suzuki, M., Okada, S., Oku, N., 2000b. ^{65}Zn localization in rat brain after intracerebroventricular injection of ^{65}Zn-histidine. Brain Res. 863, 241–244.

Tsuda, M., Imaizumi, K., Katayama, T., Kitagawa, K., Wanaka, A., Tohyama, M., Takagi, T., 1997. Expression of zinc transporter gene, ZnT-1, is induced after transient forebrain ischemia in the gerbil. J. Neurosci. 17, 6678–6684.

Valente, T., Auladell, C., Pérez-Clausell, J., 2002. Postnatal development of zinc-rich terminal fields in the brain of the rat. Exp. Neurol. 174, 215–229.

Vallee, B.L., Auld, D.S., 1993. New perspective on zinc biochemistry: cocatalytic sites in multi-zinc enzymes. Biochemistry 32, 6493–6500.

Van-Groen, T., Kiliaan, A.J., Kadish, I., 2006. Deposition of mouse amyloid beta in human APP/PS1 double and single AD model transgenic mice. Neurobiol. Dis. 23, 653–662.

Wang, Z.Y., Danscher, G., Kim, Y.K., Dahlstrom, A., Jo, S.M., 2002. Inhibitory zinc-enriched terminals in the mouse cerebellum: double-immunohistochemistry for zinc transporter 3 and glutamate decarboxylase. Neurosci. Lett. 321, 37–40.

Wang, Z.Y., Danscher, G., Dahlstrom, A., Li, J.Y., 2003. Zinc transporter 3 and zinc ions in the rodent superior cervical ganglion neurons. Neuroscience 120, 605–616.

Wang, Z.Y., Stoltenberg, M., Jo, S.M., Huang, L., Larsen, A., Dahlstrom, A., Danscher, G., 2004. Dynamic zinc pools in mouse choroid plexus. Neuroreport 15, 1801–1804.

Wang, Z.Y., Stoltenberg, M., Huang, L., Danscher, G., Dahlstrom, A., Shi, Y., Li, J.Y., 2005. Abundant expression of zinc transporters in Bergman glia of mouse cerebellum. Brain Res. Bull. 64, 441–448.

Wenzel, H.J., Cole, T.B., Born, D.E., Schwartzkroin, P.A., Palmiter, R.D., 1997. Ultrastructural localization of zinc transporter-3 (ZnT-3) to synaptic vesicle membranes within mossy fiber boutons in the hippocampus of mouse and monkey. Proc. Natl. Acad. Sci. U.S.A. 94, 12676–12681.

Wirths, O., Multhaup, G., Czech, C., Blanchard, V., Moussaoui, S., Tremp, G., Pradier, L., Beyreuther, K., Bayer, T.A., 2001. Intraneuronal Abeta accumulation precedes plaque formation in beta-amyloid precursor protein and presenilin-1 double-transgenic mice. Neurosci. Lett. 306, 116–120.

Yu, Y.Y., Kirschke, C.P., Huang, L., 2007. Immunohistochemical analysis of ZnT1, 4, 5, 6, and 7 in the mouse gastrointestinal tract. J. Histochem. Cytochem. 55, 223–234.